Recognition of modification status on a histone H3 tail by linked histone reader modules of the epigenetic regulator UHRF1

Kyohei Arita[a], Shin Isogai[a], Takashi Oda[b], Motoko Unoki[c], Kazuya Sugita[a], Naotaka Sekiyama[a], Keiko Kuwata[d], Ryuji Hamamoto[e], Hidehito Tochio[a], Mamoru Sato[b], Mariko Ariyoshi[f,g,1], and Masahiro Shirakawa[a,h,1]

[a]Department of Molecular Engineering, Graduate School of Engineering, Kyoto University, Kyoto, 615-8510, Japan; [b]Division of Macromolecular Crystallography, Graduate School of Nanobioscience, Yokohama City University, Yokohama 230-0045, Japan; [c]Division of Epigenomics, Department of Molecular Genetics, Medical Institute of Bioregulation, Kyushu University, Fukuoka 812-8582, Japan; [d]Department of Synthetic Chemistry and Biological Chemistry, Graduate School of Engineering, Kyoto University, Kyoto 615-8510, Japan; [e]Laboratory of Molecular Medicine, Human Genome Center, Institute of Medical Science, University of Tokyo, Tokyo 108-8639, Japan; [f]Institute for Integrated Cell-Material Sciences, Kyoto University, Kyoto 606-8501, Japan; and [g]Precursory Research for Embryonic Science and Technology (PREST) and [h]Core Research of Evolution Science (CREST), Japan Sciences and Technology Agency, Tokyo 102-0076, Japan

Edited by Timothy J. Richmond, Swiss Federal Institute of Technology, Zurich, Switzerland, and approved June 26, 2012 (received for review March 2, 2012)

Multiple covalent modifications on a histone tail are often recognized by linked histone reader modules. UHRF1 [ubiquitin-like, containing plant homeodomain (PHD) and really interesting new gene (RING) finger domains 1], an essential factor for maintenance of DNA methylation, contains linked two-histone reader modules, a tandem Tudor domain and a PHD finger, tethered by a 17-aa linker, and has been implicated to link histone modifications and DNA methylation. Here, we present the crystal structure of the linked histone reader modules of UHRF1 in complex with the amino-terminal tail of histone H3. Our structural and biochemical data provide the basis for combinatorial readout of unmodified Arg-2 (H3-R2) and methylated Lys-9 (H3-K9) by the tandem tudor domain and the PHD finger. The structure reveals that the intermodule linker plays an essential role in the formation of a histone H3–binding hole between the reader modules by making extended contacts with the tandem tudor domain. The histone H3 tail fits into the hole by adopting a compact fold harboring a central helix, which allows both of the reader modules to simultaneously recognize the modification states at H3-R2 and H3-K9. Our data also suggest that phosphorylation of a linker residue can modulate the relative position of the reader modules, thereby altering the histone H3–binding mode. This finding implies that the linker region plays a role as a functional switch of UHRF1 involved in multiple regulatory pathways such as maintenance of DNA methylation and transcriptional repression.

epigenetics | multidomain structure | posttranslational modification | X-ray crystallography

Various modifications such as methylation, phosphorylation, acetylation, and ubiquitination occur at residues in the amino- and carboxyl-terminal tails of core histones (1, 2). Together with cytosine methylation of genomic DNA, such histone modifications regulate various chromatin-template processes in mammals (3, 4). The presence or absence of histone modifications, referred to as "marks" hereafter, is thought to act in concert, and combinations of specific marks function as "codes" that recruit distinct complexes to regulate chromatin states (5–7). Many of the major marks form clusters on histone tails, which have been proposed to function as "modification cassettes" (5). The N terminus of histone H3 has cassettes 1 and 2, consisting of R2-K4 and K9-T11, respectively, which are subject to major modifications (5). Biological readout of a histone code made up of multiple modification cassettes is thought to require the multivalent binding of linked histone "reader" modules (5, 7, 8).

A number of histone reader modules such as plant homeodomain (PHD) fingers, bromodomains, and chromodomains have been identified in chromatin-regulation factors, and structural information on each type of module is widely available. More recent structural studies have highlighted the combinatorial read out of multiple histone marks by single or tandemly arranged reader modules (7, 9–12). However, information on the structural basis for cooperative recognition of histone marks by linked heterologous modules is still limited (8).

The patterns of histone marks and DNA methylation are cooperatively established and inherited during the cell cycle (13). A multidomain protein, UHRF1 [ubiquitin-like, containing PHD and really interesting new gene (RING) finger domains 1] (also known as Np95 or ICBP90), plays an important role in linking these two major epigenetic traits. The SRA [su(var)3-9, enhancer-of-zeste–trithorax (SET)- and RING-associated] domain of UHRF1 binds to hemimethylated DNA generated during replication and mediates loading of the DNA methylatransferase 1 (Dnmt1) for faithful inheritance of DNA-methylation pattern (14–18). In addition to the SRA domain, UHRF1 contains linked histone reader modules, namely a tandem Tudor domain (TTD) and a PHD finger (Fig. 1*A*). The isolated PHD finger and TTD recognize the methylation states of Arg-2 (H3-R2) and Lys-9 (H3-K9) in the H3 tail, respectively (19–23). Stable isotope labeling by amino acids in cell culture (SILAC)-based proteomics analysis indicated that UHRF1 binds to nucleosomes containing trimethylated H3-K9 (H3-K9me3) (24). Furthermore, the linked TTD and PHD finger have been reported to cooperatively bind to histone H3-K9me3 tail (25). However, the molecular mechanism underlying the combinatorial recognition of histone H3-K9me3 tail by the linked reader modules remains unclear.

Here, we present the crystal structure of the TTD and PHD finger region of UHRF1 in complex with the H3-K9me3 peptide. The structure clearly shows that UHRF1 simultaneously recognizes nonmodified R2 and methylated K9 in a single H3 tail through the linked reader modules. Our results reveal that the spatial arrangement of the two reader modules and induced helix formation of the H3 tail are fundamental to bivalent recognition of the histone modification states by UHRF1. We show that phosphorylation of Ser-298 in the intermodule linker abrogates the bivalent UHRF1:H3 interaction by altering the relative position of the two reader modules. This finding suggests that the linker region plays a critical role not only in maintaining the

Author contributions: K.A., M.A., and M. Shirakawa designed research; K.A., S.I., T.O., K.S., N.S., and K.K. performed research; K.A., S.I., T.O., M.U., H.T., M. Sato, and M.A. analyzed data; and K.A., M.U., R.H., M. Sato, M.A., and M. Shirakawa wrote the paper.

The authors declare no conflict of interest.

This article is a PNAS Direct Submission.

Data deposition: The atomic coordinates and structure factors have been deposited in the Protein Data Bank, www.pdb.org [PDB ID codes 3ASL (PHD:H3) and 3ASK (TTD-PHD:H3)].

[1]To whom correspondence may be addressed. E-mail: ariyoshi@moleng.kyoto-u.ac.jp or shirakawa@moleng.kyoto-u.ac.jp.

This article contains supporting information online at www.pnas.org/lookup/suppl/doi:10.1073/pnas.1203701109/-/DCSupplemental.

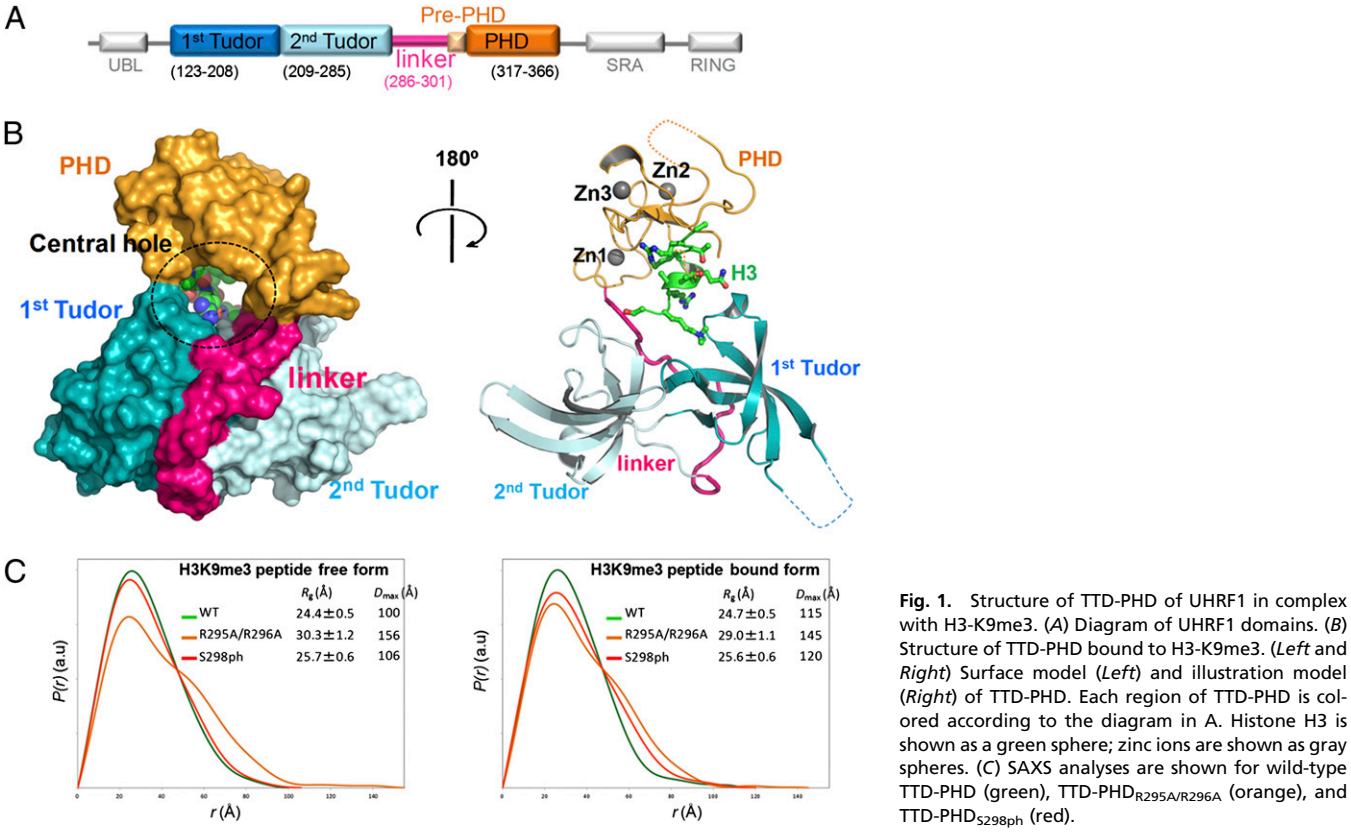

Fig. 1. Structure of TTD-PHD of UHRF1 in complex with H3-K9me3. (*A*) Diagram of UHRF1 domains. (*B*) Structure of TTD-PHD bound to H3-K9me3. (*Left* and *Right*) Surface model (*Left*) and illustration model (*Right*) of TTD-PHD. Each region of TTD-PHD is colored according to the diagram in A. Histone H3 is shown as a green sphere; zinc ions are shown as gray spheres. (*C*) SAXS analyses are shown for wild-type TTD-PHD (green), TTD-PHD$_{R295A/R296A}$ (orange), and TTD-PHD$_{S298ph}$ (red).

higher-order structure of the reader modules but also in regulation of multiple functions of UHRF1.

Results

Structure of the Linked TTD and PHD Histone Reader Modules Bound to the Histone H3 Tail. The linked histone reader modules of UHRF1 (designated "TTD-PHD" hereafter) consist of the N-terminal TTD and the C-terminal PHD finger separated by a 17-aa intermodule linker (Fig. 1*A*). In agreement with previous reports (19, 20, 23, 25), our binding assay using isothermal titration calorimetry (ITC) showed that isolated TTD and PHD bound to the N-terminal H3 peptide depending on K9me3 and unmodified R2, respectively (Table 1 and *SI Appendix*, *SI Results*). We also observed 1:1 stoichiometric binding of TTD-PHD to the H3 tail bearing unmodified R2 and K9me3 with significantly higher affinity (K_d = 0.37 μM) compared with TTD (K_d = 1.75 μM) or PHD finger (K_d = 1.47 μM) alone (Table 1 and *SI Appendix*, Fig. S3).

To understand the molecular basis for bivalent recognition of the H3 tail by UHRF1, we determined the 2.9-Å crystal structure of TTD-PHD (residues 134–366, deleting residues 167–175) in a complex with a single N-terminal H3-K9me3 tail (residues 1–12) (*SI Appendix*, Table S1). The crystal structure of the isolated PHD finger bound to the unmodified H3 tail was also solved at 1.4 Å (*SI Appendix*, Fig. S5, Table S1, and *SI Results*). The entire structure of TTD in the complex is essentially identical to that of isolated TTD (23) (Fig. 1*B* and *SI Appendix*, Fig. S6*B*). The structure of the PHD finger in TTD-PHD was nearly identical to that in the PHD:H3 complex (*SI Appendix*, Figs. S5 and S6*A* and *SI Results*). In the TTD-PHD:H3-K9me3 complex, TTD and the PHD finger are adjacent to each other, forming a ring-shaped architecture with a central hole between the modules (Fig. 1*B*). The association of modules is maintained by extensive contacts between TTD and the intermodule linker (Fig. 1*B*). The extended linker is packed against a cleft between the two Tudor domains in TTD, except for its three C-terminal residues (299–301), which serves as an intermodule junction between the two reader modules (see Fig. 4*A*). No apparent interface is observed between the TTD and PHD finger, indicating the importance of the conformation of the linker for maintaining the higher-order structure of TTD-PHD (Fig. 1*B*). The *P*(*r*) function obtained from small-angle X-ray scattering (SAXS) measurements of the TTD-PHD:H3-K9me3 complex showed broader distribution to some extent than that calculated from the crystal structure (*SI Appendix*, Fig. S4*C*). Therefore, it is not likely that the domain orientation is static in solution, which is consistent with poor electron density of PHD fingers observed in two of four complexes in the crystal asymmetric unit (*SI Appendix*, Fig. S12 *A–C* and *SI Results*). In addition, the free and H3-bound forms showed overall similar *P*(*r*) profiles, suggesting that the ring-shaped architecture of TTD-PHD and its intrinsic dynamic motion are mainly defined by the structure around the intermodular junction rather than by the H3 binding (Fig. 1*C* and *SI Appendix*, Fig. S4 *A* and *B* and *SI Results*).

Specific Recognition of the Histone H3 Tail by TTD-PHD. The PHD finger and TTD make dense contacts with two stretches of histone H3 from A1 to K4 in cassette 1 and from K9me3 to S10 in cassette 2, respectively, at the inner walls of the negatively charged central hole (Fig. 2*A*). Binding of the H3-K9me3 tail to TTD-PHD excludes about 650 Å^2 of solvent accessible area on the TTD-PHD surface, which is provided equally by TTD and the PHD finger.

The H3 recognition mode of the isolated PHD finger is well-conserved in the TTD-PHD:H3-K9me3 complex (Fig. 2*B* and *SI Appendix*, Fig. S5*B*) (19, 20). Residues 2–4 of H3 cassette 1 make main-chain hydrogen bonds to form an intermolecular β-sheet with the PHD finger (residues 330–333) (Fig. 2*B* and *SI Appendix*, Fig. S7). The N-terminal amino group of the H3 tail donates direct hydrogen bonds to the backbone carbonyl oxygens of E355 and D356 of the PHD finger (Fig. 2*B* and *SI Appendix*, Fig. S7 and *SI Results*). The side chain of H3-R2 fits into the acidic cavity in the PHD finger, in which the guanidino nitrogen atoms are strictly recognized by hydrogen bonds with the UHRF1 residues, C333, D334, and D337 (Fig. 2*B* and *SI Appendix*, Fig. S7). Indeed,

Table 1. Summary of ITC measurements

Histone and protein	K_d (μM)	ΔH (kcal/mol)	N*
H3-K9me3			
PHD	1.47 ± 0.07	−6.36 ± 0.30	1.02 ± 0.04
TTD	1.75 ± 0.19	−8.35 ± 0.06	1.17 ± 0.08
TTD-PHD	0.37 ± 0.01	−12.10 ± 0.67	1.00 ± 0.05
R295A/R296A[†]	3.27 ± 0.17[‡]	−8.22 ± 0.05	2.06 ± 0.04
S298ph[§]	8.99 ± 0.65[‡]	−10.52 ± 0.11	1.49 ± 0.06
TTD+PHD[¶]	1.99 ± 0.28[‡]	−8.27 ± 0.28	2.16 ± 0.01
Unmodified H3			
PHD	1.73 ± 0.09	−6.89 ± 0.07	0.99 ± 0.01
TTD	N/D[‖]	N/D	N/D
TTD-PHD	1.04 ± 0.20	−6.94 ± 0.57	1.02 ± 0.05
H3-R2me2a**			
PHD	12.70 ± 1.57	−3.22 ± 0.11	0.97 ± 0.02
TTD-PHD	10.29 ± 2.93	−4.41 ± 0.26	0.91 ± 0.04
H3-R2me2-K9me3			
TTD	1.98 ± 0.82	−7.41 ± 0.70	−1.17 ± 0.05
TTD-PHD	3.43 ± 0.02	−8.05 ± 0.19	−1.05 ± 0.02
H3-T3ph-K9me3			
PHD	N/D	N/D	N/D
TTD	6.66 ± 0.51	−6.51 ± 0.16	1.12 ± 0.01
TTD-PHD	N/D	N/D	N/D
H3-K9me3-S10ph			
PHD	2.69 ± 0.22	−5.90 ± 0.13	0.99 ± 0.01
TTD	5.81 ± 0.89	−7.20 ± 0.42	1.16 ± 0.02
TTD-PHD	2.50 ± 0.13	−6.14 ± 0.11	1.04 ± 0.05
H3-A1ac[††]-K9me3			
PHD	N/D	N/D	N/D
TTD	1.79 ± 0.61	−8.34 ± 0.58	1.15 ± 0.02
TTD-PHD	N/D	N/D	N/D

N/D, not detected.
*Binding stoichiometry.
[†]Arg-295 and Arg-296 substituted to alanine in TTD-PHD.
[‡]Because the binding stoichiometry was not 1:1 or could not be determined from the ITC data, the apparent dissociation constants calculated on the basis of an assumption of 1:1 stoichiometry are not accurate.
[§]Phosphorylated Ser-298 in TTD-PHD.
[¶]An equimolar mixture of isolated TTD and PHD finger was the titrant.
[‖]No or very weak binding was observed in the ITC experiment.
**N^G-N^G asymmetric dimethylated arginine.
[††]Acetylation of N-terminal amide.

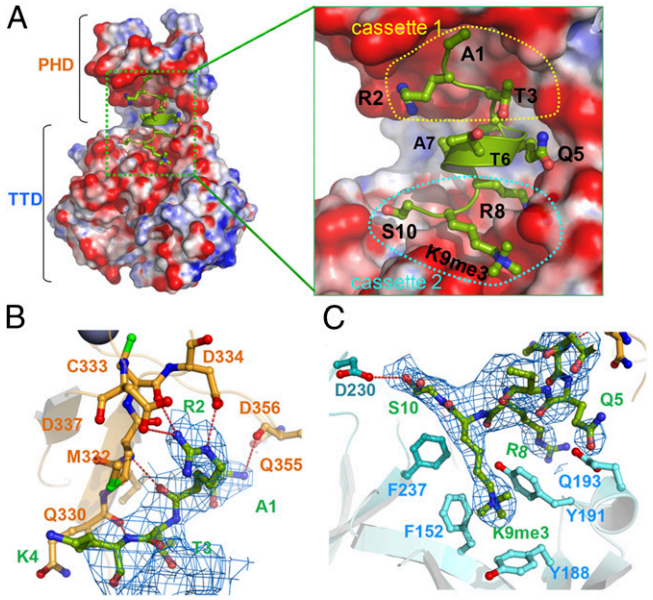

Fig. 2. Recognition of histone H3-K9me3 by UHRF1. (*A*) Electrostatic surface potential of TTD-PHD. Surface colors represent the potential from −15 K_BT^{-1} (red) to 15 K_BT^{-1} (blue). Histone H3-K9me3 is shown by a ball-and-stick model. (*Right*) Close-up view of $H3_{1–10}$, fitting into the hole of TTD-PHD. (*B*) Recognition of the cassette 1 region of histone H3 by TTD-PHD. Selected residues involved in the TTD-PHD:H3 interfaces are indicated. The color coding is the same as in Fig. 1*A*. Red dotted lines indicate hydrogen bonds. The $2|F_o| - |F_c|$ difference Fourier map for histone H3 (>1.0 σ) is shown in blue. (*C*) Recognition of the cassette 2 region of the histone H3 tail. The residues of TTD-PHD involved in histone H3 recognition are shown as a cyan stick model, with nitrogen and oxygen atoms in blue and red, respectively.

methylation of H3-R2 decreased the binding affinity of the isolated PHD finger for the unmodified H3 peptide (K_d = 12.70 μM) and also interfered with the interaction of H3 with TTD-PHD regardless of H3-K9 methylation (Table 1). In the isolated TTD:H3-K9me3 complex, the cleft between the Tudor domain accommodates the side chain of H3-K4 (23), whereas in the TTD-PHD:H3K9me3 complex, the same region forms an extended interface with the inter modular linker (Fig. 1*B*). No significant interaction between the H3-K4 side chain and protein residues is observed in the TTD-PHD:H3K9me3 complex (Fig. 2*C*). Thus, the H3-binding mode of isolated TTD does not represent that in the context of the linked TTD-PHD.

The C-terminal two residues in cassette 2, H3-K9me3 and H3-S10, form contacts only with the first Tudor domain region. The aliphatic side chain of K9me3 fits into a surface groove, and the trimethyl ammonium group is trapped in an "aromatic cage" motif formed by F152, Y188, and Y191 of the first Tudor domain (Fig. 2*C* and *SI Appendix*, Fig. S7), as commonly observed for other methylated lysines in reader modules (7, 26). The hydroxyl group of H3-S10 donates a hydrogen atom to the carboxyl group of D230 of UHRF1, which is not observed in the structure of the TTD:H3 complex (Fig. 2*C* and *SI Appendix*, Fig. S6*B*). No binding of isolated TTD to the unmodified H3 tail was observed in the ITC-binding assay. Nonmethylation of H3-K9 decreased the affinity of TTD-PHD for H3 down to the same order as that of the isolated PHD finger (Table 1). TTD-PHD simultaneously recognizes unmodified R2 in cassette 1 and K9me3 in cassette 2 on a single histone H3 tail.

Induced Helix Formation of the Histone H3 Tail. In contrast to the cassette regions, residues 5–8 of the H3 tail make no amino acid–specific contacts with TTD-PHD and form an α-helix stabilized by an N-capping hydrogen bond between T3 Oγ and T6 NH (Fig. 3*A*). The same segment in the isolated PHD:H3 complex adopts an extended conformation (*SI Appendix*, Fig. S5); thus, the helix formation seems to be induced by the bivalent interaction with TTD-PHD. This conformational change upon binding to TTD-PHD was confirmed by comparison of the ^1H-^{15}N correlation spectra of the ^{13}C, ^{15}N-labeled H3-K9me3 peptide in its free and bound forms (Fig. 3*A*). We assigned the chemical shifts of the backbone ^1HN, ^{15}N, $^{13}C_\alpha$, and ^{13}CO nuclei of the H3-K9me3 peptide in complex with TTD-PHD, except for A1, K4, Q5, and K9me3, and its secondary structure was predicted on the basis of its backbone $^{13}C_\alpha$ and ^{13}CO chemical shifts. In agreement with the crystal structure, at least residues 6–8 are suggested to form an α-helix, whereas the C-terminal residues 11–20 are structurally random (Fig. 3 *A* and *B*). Such a helical conformation in the H3 tail has not been observed in other histone-binding complexes (7, 26), except that a $H3_{1–16}$ tail–like peptide inhibitor bound to lysine specific demethylase 1 (LSD1), which bears Met in place of H3-K4, has been reported to form a similar helical structure (27).

On basis of the structural findings, we reasoned that modification of the H3 tail with negative charge, such as phosphorylation, would have a negative effect on its interaction with TTD-PHD. The ITC data showed that phosphorylation of H3-T3 or H3-S10 significantly repressed binding of TTD-PHD to the H3-K9me3 tail (Table 1). Thus, both the shape and charge complementarities are important for TTD-PHD:H3 interactions (Fig. 2*A*).

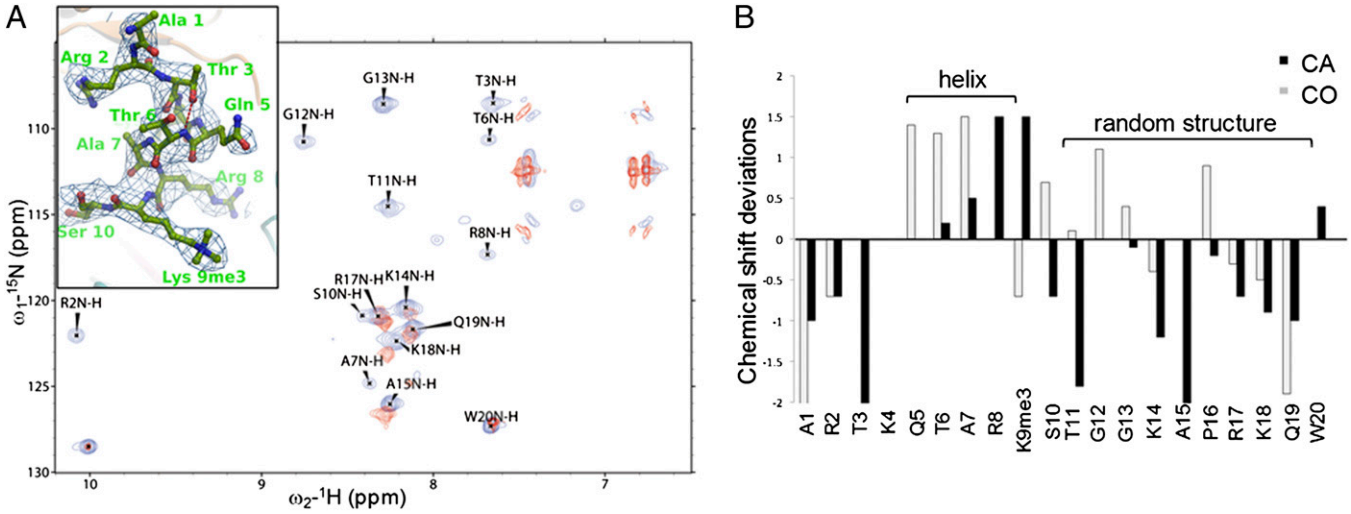

Fig. 3. Structure of the histone H3 tail. (*A*) Overlay of the ^{1}H-^{15}N correlation spectra of the histone H3 tail (residues 1–20, containing the K9me3 analog) alone and bound to wild-type TTD-PHD in red and blue, respectively. Structure of the H3-K9me3 peptide superimposed on the $2|F_o| - |F_c|$ difference Fourier map contoured at 1.0 σ (blue) is depicted in the box. (*B*) Chemical shift deviations of ^{13}CA and ^{13}CO from the random coil values in the histone H3-K9me3 peptide.

Linker:Tudor Contacts Define the Histone H3–Binding Mode of TTD-PHD. The structural importance of the TTD:linker contacts was further assessed by SAXS analysis using a linker mutant (TTD-PHD$_{R295A/R296A}$), in which residues R295 and R296, whose side chains make contacts with TTD (Fig. 4*A*), were substituted with alanine. TTD-PHD$_{R295A/R296A}$ exhibited a $P(r)$ distribution with a shoulder, which is a characteristic of noncompact flexible proteins composed of two domains (Fig. 1*C*). This $P(r)$ distribution, which deviated from that of the wild type, was observed regardless of H3 binding (Fig. 1*C*). Combined with the results of NMR experiments (*SI Appendix*, Fig. S8), these data suggest that the R295A/R296A mutations disrupt the compact ring-shape structure.

TTD-PHD$_{R295A/R296A}$ bound the H3-K9me3 tail with an affinity ∼10-fold lower than that of the wild type and with an N value of 2.06, which suggests loss of the 1:1 stoichiometric interaction (Fig. 4*B* and Table 1). Furthermore, in the ^{1}H-^{15}N correlation spectrum of the H3-K9me3 peptide bound to TTD-PHD$_{R295A/R296A}$, the chemical shifts presumably attributed to

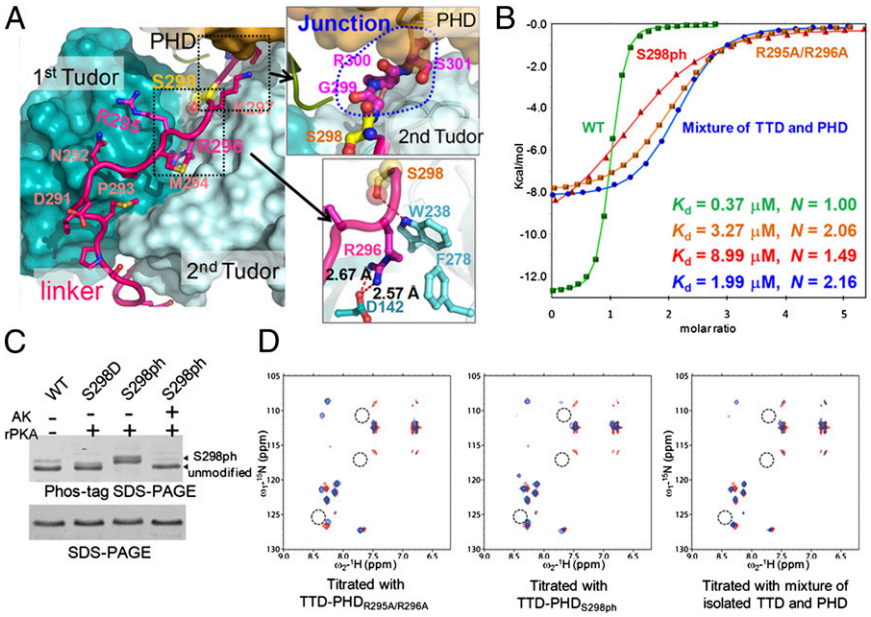

Fig. 4. Disruption of the linker:Tudor contacts alters the binding mode of TTD-PHD to the histone H3 tail. (*A*) Contacts between the linker and TTD. The side chains of the linker residues are shown as ball-and-stick models in magenta. The space-filling model in yellow indicates S298. (*Upper Right* and *Lower Right*) Close-up views of the intermodule junction (*Upper Right*) and the interactions (*Lower Right*) between the linker and TTD. (*B*) ITC measurements of wild-type TTD-PHD, TTD-PHD$_{R295A/R296A}$, TTD-PHD$_{S298ph}$, and an equimolar mixture of isolated TTD and PHD finger with H3-K9me3 peptide. The integrated heat of each injection is depicted. The ITC thermograms of all experiments are shown in *SI Appendix*, Figs. S1–S3. (*C*) Phosphorylation of TTD-PHD S298 in *E. coli*. Phosphorylation by rPKA was confirmed by a gel shift-mobility assay using phos-tag SDS/PAGE. The total amount of protein in each lane was 0.3 μg. AK indicates alkaline phosphatase treatment to remove a phosphate group. (*D*) ^{1}H-^{15}N correlation spectrum of H3-K9me3 peptide alone (red) overlaid with that in the presence of a 2-molar excess of TTD-PHD$_{R295A/R296A}$, TTD-PHD$_{S298ph}$, or an equimolar mixture of the isolated TTD and PHD finger (blue). The dotted circle shows the peaks of residues T6-R8 of H3, which are representative peaks of helical structure in the complex with wild-type TTD-PHD.

helix formation were not observed (Figs. 3*B* and 4*D*). Notably, the interaction of the linker mutant with the H3-K9me3 tail exhibited thermodynamic parameters similar to those calculated from titration with an equimolar solution of the isolated TTD and PHD finger (Fig. 4*B* and Table 1). This is consistent with the NMR spectrum of the H3-K9me3 peptide bound to TTD-PHD$_{R295A/R296A}$, which was superimposed on those of the peptide titrated with isolated TTD and PHD finger (Fig. 4*D*), These data suggest that the R295A/R296A mutations abrogate the simultaneous binding of TTD-PHD to H3-R2 and H3-K9me3, resulting in an independent H3-binding mode of each reader module.

Phosphorylation of S298 at the Linker Region in UHRF1. S298, which is located at the junction and contacts the indole ring of W238 on the surface of TTD (Fig. 4*A*), is a target of PKA phosphorylation (28). The corresponding phosphorylation site in homologous proteins is highly conserved among mammals, birds, and reptiles, suggesting its functional importance (*SI Appendix*, Fig. S9). We prepared TTD-PHD phosphorylated at S298 (TTD-PHD$_{S298ph}$) using a bacterial coexpression system with PKA (Fig. 4*C* and *SI Appendix*, Fig. S10 and *SI Results*) and analyzed its solution structure by SAXS. The SAXS data indicated that, unlike TTD-PHD$_{R295A/R296A}$, TTD-PHD$_{S298ph}$ exhibited only small differences from wild-type TTD-PHD in the R_g value and the profile of the $P(r)$ function (Fig. 1*C* and *SI Appendix*, Fig. S4 *A* and *B*). Comparing the ^{1}H-^{15}N correlation spectra between wild-type TTD-PHD and TTD-PHD$_{S298ph,}$ phosphorylation of S298 caused chemical shift differences in 15 signals (*SI Appendix*, Fig. S11*A*), implying local conformational changes at or near the junction. Nevertheless, phosphorylation of S298 decreased the apparent binding affinity for the H3-K9me3 tail ~30-fold and abrogated the binding stoichiometry (n = 1.49) (Fig. 4*B* and Table 1). Indeed, the NMR spectrum of the H3-K9me3 peptide bound to TTD-PHD$_{S298ph}$ did not show peaks corresponding to those of the H3 residues that presumably form the helix in the nonphosphorylated complex (Figs. 3*B* and 4*D*). Collectively, either local perturbation of the linker:TTD contacts or alteration of the junction conformation by S298ph disrupts the simultaneous recognition of multiple modifications in the histone H3 tail by TTD-PHD.

Discussion

Our structural and binding data clearly demonstrate the combinatorial recognition of methylated H3-K9 and nonmodified H3-R2 by TTD-PHD of UHRF1. The crystal structure of the TTD-PHD:H3-K9me3 complex illustrates two major fundamental structural aspects of the combinatorial recognition, which have been missing in previous structural studies of isolated TTD and PHD. One is the critical role of the intermodule linker conformation in the stoichiometric interaction with the H3-K9me3 tail. The interaction between TTD and the linker region obviously maintains a specific spatial arrangement of TTD-PHD to accomplish bivalent contacts with separated regions of histone H3 (Fig. 1*B*). Indeed, double mutation of the linker (R295A/R296A) disrupted the higher-order structure and stoichiometric H3 binding. Another important structural finding is the conformational change in the H3 tail on TTD-PHD binding. The SAXS data indicated that H3 binding causes no significant structural change in TTD-PHD (Fig. 1*C*). The simultaneous binding of H3-R2 and H3-K9me3 to PHD and TTD, therefore, appears to be facilitated by distance adjustment through α-helix formation in the H3 segment between the cassettes. Such helix formation was not observed in the H3-K9me3 tail in the presence of isolated PHD and TTD or in the presence of TTD-PHD$_{R295A/R296A}$ (Figs. 3*A* and 4*D*), suggesting its strict coupling with the higher-order structure of TTD-PHD.

UHRF1 undergoes PKA phosphorylation at S298, which is located at the junction (28). Our NMR and ITC experiments indicated that modulation of the linker:Tudor contacts by S298 phosphorylation changed the binding mode of UHRF1 to the histone H3 tail (Figs. 3*B* and 4 *B* and *D*). The modification is likely to cause only local perturbation in the linker:Tudor contacts (Fig. 1*C* and *SI Appendix*, Fig. S11). SAXS and NMR analysis of TTD-PHD$_{S298ph}$ showed that it had a smaller structural deviation from wild-type TTD-PHD compared with the linker mutant (Fig. 1*C* and *SI Appendix*, Fig. S11*A*). Phosphorylation of S298 might significantly destabilize the interfaces between TTD-PHD and the H3 tail by altering the electrostatic static distribution and/or its domain orientation. These data suggest the possibility that phosphorylation of S298 acts as a functional switch of UHRF1 that is implicated in multiple regulatory pathways such as maintenance DNA methylation, transcriptional repression, and cell cycle progression (29).

Combined with the structural data, our in vitro–binding assay showed modulation of H3 binding to TTD-PHD by other histone modifications apart from the methylation states of H3-R2 and H3-K9. For example, H3-T3 phosphorylation significantly affects the interface of both cassettes 1 and 2 with TTD-PHD (Fig. 2*A* and Table 1) and presumably destabilizes the helical structure of the H3-tail by perturbing the N-capping hydrogen bond (Fig. 3*A*). Moreover, H3-S10 phosphorylation is likely to perturb the interface between the TTD region and cassette 2 (Fig. 2*C*) and, indeed, causes a ninefold reduction in the affinity of TTD-PHD for the H3-K9me3 tail (Table 1). These data imply involvement of a methylation/phosphorylation binary switch in functional regulation of UHRF1 in a manner analogous to the binding of heterochromatin protein (HP)1α to H3-K9me that is inhibited by phosphorylation at H3-S10 (5). Notably, acetylation of the N terminus of the H3-K9me3 tail, which does not disturb the binding of TTD alone, abolishes binding to both the PHD finger and TTD-PHD (Table 1). In contrast, TTD-PHD retains affinity for the nonmethylated H3K9 peptide similar to that of the isolated PHD finger despite loss of the interaction through the TTD moiety. This manner of context-dependent binding implies synergistic binding of the linked TTD and PHD finger to the histone H3 tail. Recognition of the H3 tail by the PHD finger might be prerequisite for the efficient and/or stable binding of TTD to H3-K9me3 in the context of the linked reader modules.

Our data demonstrate how the two linked reader modules recognize distant histone modification cassettes in the histone H3 tail and, thus, provide structural evidence for the "histone code" and "modification cassette" hypotheses (5, 30). Trimethylation of histone H3K9 is well known to be associated with transcriptional suppression (31), but the role of H3-R2 methylation has just started to be unveiled (32–35). Recently, H3-R2 binding of UHRF1 was shown to be dispensable for localization of UHRF1 at pericentromeric heterochromatin (19, 20). However, the biological relevance of the histone code (H3-R2me0-K9me3) that is recognized by the TTD-PHD of UHRF1 remains to be clarified.

Methods

Protein Preparation. DNA fragments encoding the PHD finger (299–366), TTD (123–285), TTD-linker (123–300), and TTD-PHD (123–366) of human UHRF1 were each amplified by PCR and cloned into modified a pGEX4T-3 plasmid (GE Healthcare Bio-Sciences) engineered for protein expression with an N-terminal GST and small ubiquitin like modifier (SUMO)-1 fusion tag. For ITC and NMR experiments, a TTD-PHD$_{R295A/R296A}$ mutant was generated by the QuikChange method (Stratagene). We also prepared the TTD-PHD, residues 134–366, with a deletion of residues 167–175, for crystallography. Each protein was overexpressed in *Escherichia coli* strain Rosetta (DE3) and purified by affinity, ion-exchange, and size-exclusion chromatography (GE Healthcare Bio-Sciences). More details are provided in *SI Appendix, SI Methods*.

Preparation of TDD-PHD$_{S298ph}$ Using an *E. coli* Phosphorylation System. Phosphorylated TTD-PHD was prepared by coexpression with rat cAMP-dependent protein kinase (rPKA) (residues 1–350) in *E. coli* BL21 (DE3). Phosphorylation efficiency and specificity was examined by a gel shift-mobility assay using Phos-tag SDS/PAGE and liquid chromatography-electrospray ionization-tandem mass spectroscopy (LC-ESI-MS/MS) analysis. More details are provided in *SI Appendix, SI Methods* and *SI Results*.

Peptide Preparation. The histone H3 peptides H3$_{1–10}$ and H3$_{1–12}$-K9me3 for crystallography and a series of H3 peptides for ITC measurements were purchased from Toray Research Center. Histones H3$_{1–20}$ and H4 peptides harboring a site- and degree-specific methylated lysine analog were prepared by cysteine alkylation as reported previously (36, 37).

ITC Measurements. A MicroCal calorimeter, itc200, was used for the ITC measurements. Protein solutions were dialyzed into buffer [10 mM Hepes (pH 7.5), 150 mM NaCl, 0.1 mM tris(2-carboxyethyl)phosphine (TCEP), 30 μM zinc acetate], and lyophilized histone peptides were dissolved in the same buffer. All measurements were carried out at 293 K. The protein solution (30–60 μM) in the calorimetric cell was titrated with the peptide solution (400–800 μM). The data were analyzed with the software ORIGIN (MicroCal) using a one-site model. The first data point was excluded from the analysis. For each interaction, at least three independent titration experiments were performed. A summary of the ITC measurement and results is given in *SI Appendix*, Table S2 and Figs. S1–S3.

X-Ray Crystallography of TTD-PHD in Complex with the H3-K9me3 Peptide. TTD-PHD (residues 123–366), with residues 123–132 deleted in the N-terminal region and 167–175 deleted in a loop region, was used for crystallization. The TTD-PHD:H3 complex was prepared by adding a 1.5-molar excess of $H3_{1-12}$K9me3 peptide to the protein before concentration. The crystal was obtained by using a 20 mg/mL concentration of the complex at 4 °C and the hanging drop vapor diffusion method with a reservoir solution containing 100 mM Bis-Tris propane (pH 6.5), 200 mM sodium citrate, and 20% PEG3350. The crystal was directly frozen in liquid nitrogen using a cryoprotectant containing 20% (vol/vol) ethylene glycol. The X-ray diffraction data were collected at a wavelength of 1.0000 Å on an ADSC Q315 CCD detector in beamline BL-5A at Photon Factory (PF) (Tsukuba, Japan) and scaled at 2.9 Å resolution with the program HKL2000 (38). The structure was solved by molecular replacement using the coordinates of TTD (PDB ID code 3db3) and the PHD finger of UHRF1 as search models. After several cycles of refinement by the program PHENIX (39) with noncrystallographic symmetry restraints in the four TTD moieties, the model was converged, resulting in a crystallographic *R* value of 24.2% and a free *R* value of 28.6% for all diffraction data up to 2.9-Å resolution. Four TTD-PHD complexes, designated as complexes A, B, C, and D, are included in an asymmetric unit and show different average temperature factors, in particular for the PHD moiety (see *SI Appendix*, *SI Results* and *SI Methods*). The structure of complex A is described in the main text. The peptide bond between Gly-299 and Pro-300 in molecules A and B is in the *cis* conformation. The crystallographic data and refinement statistics are given in *SI Appendix*, Table S1. More details are provided in *SI Appendix*.

SAXS. SAXS measurements were performed with a Rigaku NANO-VIEWER system mounted on a Rigaku FR-D X-ray generator. The scattering intensities were recorded with a PILATUS 100K detector. SAXS data were analyzed with the software package ATSAS 2.4. The radius of gyration R_g was estimated from the Guinier plot (40) of $I(q)$. The distance distribution function $P(r)$ was calculated in the program GNOM (41). More details are provided in *SI Appendix*, *SI Methods*.

NMR Spectroscopy. The ^{1}H-^{15}N band-selective optimized-flip-angle-short-transient (SOFAST)–heteronuclear multiple quantum coherence (HMQC) spectra (42) of wild-type TTD-PHD, TTD-PHD$_{R295A/R296A}$, TTD-PHD$_{S298ph}$, TTD, TTD linker, and PHD finger were acquired at 30 °C on a Bruker DRX-700 spectrometer equipped with a TCI cryogenic probe. To assign the backbone ^{1}NH, ^{15}N, $^{13}C_{\alpha}$, and ^{13}CO chemical shifts of the H3-K9me3 peptide, ^{1}H-^{15}N heteronuclear single quantum coherence (HSQC), HNCO, HNCA, and HN(CO)CA spectra were measured with a Bruker Avance 800-MHz spectrometer equipped with a TCI cryogenic probe at 30 °C. More details are provided in *SI Appendix*, *SI Methods* and *SI Results*.

ACKNOWLEDGMENTS. We thank Drs. Y. Nakamura and S. Tajima for discussions; Dr. T. Kokubo for comments on the manuscript; Drs. A. Ojida and I. Hamachi for their help in recording ITC data; Drs. N. Matsugaki, N. Igarashi, and Y. Yamada and Prof. S. Wakatsuki for data collection at Photon Factory (PF); and Dr. S. Tajima for providing a cDNA of rat PKA. This work was supported by grants from the Ministry of Education, Culture, Sports, Science and Technology (MEXT) and the Japan Science and Technology Agency (JST) (to M.S.); by a Grant-in-Aid for Scientific Research (A) and Grant-in-Aid for Scientific Research on Innovative Areas from the Japan Society for the Promotion of Science (to K.A.); by JST, Precursory Research for Embryonic Science and Technology (PREST) (to M.A.); and, in part, by the Global Centers of Excellence (COE) Program "International Center for Integrated Research and Advanced Education in Materials Science" (B-09) of MEXT, administered by the Japan Society for the Promotion of Science.

1. Roth SY, Allis CD (1996) Histone acetylation and chromatin assembly: A single escort, multiple dances? *Cell* 87:5–8.
2. Cheung P, Allis CD, Sassone-Corsi P (2000) Signaling to chromatin through histone modifications. *Cell* 103:263–271.
3. Jenuwein T, Allis CD (2001) Translating the histone code. *Science* 293:1074–1080.
4. Bird A (1992) The essentials of DNA methylation. *Cell* 70:5–8.
5. Fischle W, Wang Y, Allis CD (2003) Binary switches and modification cassettes in histone biology and beyond. *Nature* 425:475–479.
6. Schones DE, Zhao K (2008) Genome-wide approaches to studying chromatin modifications. *Nat Rev Genet* 9:179–191.
7. Taverna SD, Li H, Ruthenburg AJ, Allis CD, Patel DJ (2007) How chromatin-binding modules interpret histone modifications: Lessons from professional pocket pickers. *Nat Struct Mol Biol* 14:1025–1040.
8. Ruthenburg AJ, Li H, Patel DJ, Allis CD (2007) Multivalent engagement of chromatin modifications by linked binding modules. *Nat Rev Mol Cell Biol* 8:983–994.
9. Zeng L, et al. (2010) Mechanism and regulation of acetylated histone binding by the tandem PHD finger of DPF3b. *Nature* 466:258–262.
10. Tsai WW, et al. (2010) TRIM24 links a non-canonical histone signature to breast cancer. *Nature* 468:927–932.
11. Ruthenburg AJ, et al. (2011) Recognition of a mononucleosomal histone modification pattern by BPTF via multivalent interactions. *Cell* 145:692–706.
12. Iwase S, et al. (2011) ATRX ADD domain links an atypical histone methylation recognition mechanism to human mental-retardation syndrome. *Nat Struct Mol Biol* 18:769–776.
13. Cedar H, Bergman Y (2009) Linking DNA methylation and histone modification: Patterns and paradigms. *Nat Rev Genet* 10:295–304.
14. Bostick M, et al. (2007) UHRF1 plays a role in maintaining DNA methylation in mammalian cells. *Science* 317:1760–1764.
15. Sharif J, et al. (2007) The SRA protein Np95 mediates epigenetic inheritance by recruiting Dnmt1 to methylated DNA. *Nature* 450:908–912.
16. Arita K, Ariyoshi M, Tochio H, Nakamura Y, Shirakawa M (2008) Recognition of hemi-methylated DNA by the SRA protein UHRF1 by a base-flipping mechanism. *Nature* 455:818–821.
17. Avvakumov GV, et al. (2008) Structural basis for recognition of hemi-methylated DNA by the SRA domain of human UHRF1. *Nature* 455:822–825.
18. Hashimoto H, et al. (2008) The SRA domain of UHRF1 flips 5-methylcytosine out of the DNA helix. *Nature* 455:826–829.
19. Wang C, et al. (2011) Structural basis for site-specific reading of unmodified R2 of histone H3 tail by UHRF1 PHD finger. *Cell Res* 21:1379–1382.
20. Rajakumara E, et al. (2011) PHD finger recognition of unmodified histone H3R2 links UHRF1 to regulation of euchromatic gene expression. *Mol Cell* 43:275–284.
21. Karagianni P, Amazit L, Qin J, Wong J (2008) ICBP90, a novel methyl K9 H3 binding protein linking protein ubiquitination with heterochromatin formation. *Mol Cell Biol* 28:705–717.
22. Rottach A, et al. (2010) The multi-domain protein Np95 connects DNA methylation and histone modification. *Nucleic Acids Res* 38:1796–1804.
23. Nady N, et al. (2011) Recognition of multivalent histone states associated with heterochromatin by UHRF1 protein. *J Biol Chem* 286:24300–24311.
24. Bartke T, et al. (2010) Nucleosome-interacting proteins regulated by DNA and histone methylation. *Cell* 143:470–484.
25. Xie S, Jakoncic J, Qian C (2012) UHRF1 double tudor domain and the adjacent PHD finger act together to recognize K9me3-containing histone H3 tail. *J Mol Biol* 415:318–328.
26. Adams-Cioaba MA, Min J (2009) Structure and function of histone methylation binding proteins. *Biochem Cell Biol* 87:93–105.
27. Forneris F, Binda C, Adamo A, Battaglioli E, Mattevi A (2007) Structural basis of LSD1-CoREST selectivity in histone H3 recognition. *J Biol Chem* 282:20070–20074.
28. Trotzier MA, et al. (2004) Phosphorylation of ICBP90 by protein kinase A enhances topoisomerase IIalpha expression. *Biochem Biophys Res Commun* 319:590–595.
29. Unoki M, Brunet J, Mousli M (2009) Drug discovery targeting epigenetic codes: The great potential of UHRF1, which links DNA methylation and histone modifications, as a drug target in cancers and toxoplasmosis. *Biochem Pharmacol* 78:1279–1288.
30. Strahl BD, Allis CD (2000) The language of covalent histone modifications. *Nature* 403:41–45.
31. Lachner M, O'Carroll D, Rea S, Mechtler K, Jenuwein T (2001) Methylation of histone H3 lysine 9 creates a binding site for HP1 proteins. *Nature* 410:116–120.
32. Kirmizis A, et al. (2009) Distinct transcriptional outputs associated with mono- and dimethylated histone H3 arginine 2. *Nat Struct Mol Biol* 16:449–451.
33. Kirmizis A, et al. (2007) Arginine methylation at histone H3R2 controls deposition of H3K4 trimethylation. *Nature* 449:928–932.
34. Wang Z, et al. (2008) Combinatorial patterns of histone acetylations and methylations in the human genome. *Nat Genet* 40:897–903.
35. Migliori V, et al. (2012) Symmetric dimethylation of H3R2 is a newly identified histone mark that supports euchromatin maintenance. *Nat Struct Mol Biol* 19:136–144.
36. Simon MD, et al. (2007) The site-specific installation of methyl-lysine analogs into recombinant histones. *Cell* 128:1003–1012.
37. Otani J, et al. (2009) Structural basis for recognition of H3K4 methylation status by the DNA methyltransferase 3A ATRX-DNMT3-DNMT3L domain. *EMBO Rep* 10:1235–1241.
38. Otwinowski Z, Minor W (1997) Processing of X-ray diffraction data collected in oscillation mode. *Methods Enzymol* 276:307–326.
39. Adams PD, et al. (2002) PHENIX: Building new software for automated crystallographic structure determination. *Acta Crystallogr D Biol Crystallogr* 58:1948–1954.
40. Glatter O, Kratky O (1982) *Small-Angle X-Ray Scattering* (Academic, New York).
41. Svergun DI (1992) Determination of the regularization parameter in indirect-transform methods using perceptual criteria. *J Appl Cryst* 25:495–503.
42. Schanda P, Brutscher B (2005) Very fast two-dimensional NMR spectroscopy for real-time investigation of dynamic events in proteins on the time scale of seconds. *J Am Chem Soc* 127:8014–8015.